



Original Article

A comparative study of machine learning methods for automated identification of radioisotopes using NaI gamma-ray spectra

S.M. Galib^a, P.K. Bhowmik^a, A.V. Avachat^a, H.K. Lee^{b,*}^a Department of Nuclear Engineering and Radiation Science, Missouri University of Science and Technology, 1201 N. State St., Rolla, MO, 65409, USA^b Department of Nuclear Engineering, University of New Mexico, Albuquerque, NM 87131, USA

ARTICLE INFO

Article history:

Received 27 March 2021

Received in revised form

27 May 2021

Accepted 12 June 2021

Available online 20 June 2021

Keywords:

Artificial neural network

Gamma-ray spectroscopy

Radioisotope identification

Real-time processing

Nuclear security

Nuclear threat detection

ABSTRACT

This article presents a study on the state-of-the-art methods for automated radioactive material detection and identification, using gamma-ray spectra and modern machine learning methods. The recent developments inspired this in deep learning algorithms, and the proposed method provided better performance than the current state-of-the-art models. Machine learning models such as: fully connected, recurrent, convolutional, and gradient boosted decision trees, are applied under a wide variety of testing conditions, and their advantage and disadvantage are discussed. Furthermore, a hybrid model is developed by combining the fully-connected and convolutional neural network, which shows the best performance among the different machine learning models. These improvements are represented by the model's test performance metric (i.e., F1 score) of 93.33% with an improvement of 2%–12% than the state-of-the-art model at various conditions. The experimental results show that fusion of classical neural networks and modern deep learning architecture is a suitable choice for interpreting gamma spectra data where real-time and remote detection is necessary.

© 2021 Korean Nuclear Society, Published by Elsevier Korea LLC. This is an open access article under the CC BY-NC-ND license (<http://creativecommons.org/licenses/by-nc-nd/4.0/>).

1. Introduction

Automatic radioisotope identification in real-time is important in a wide variety of applications, including prevention of nuclear terrorism [1–3], monitoring of environmental contamination [4–7], and analysis of medical data [8]. Different types of radioactive materials may require screening during a radiological search operation. These include Special Nuclear Materials (SNM) (e.g., high enriched uranium and weapons-grade plutonium), medical isotopes (e.g., patients recently treated with radiation/nuclear medicine may contain Iodine-131 or Technetium-99), industrial isotopes (e.g., Cobalt-60 and Selenium-75 are used for gamma radiography and non-destructive testing), and Naturally Occurring Radioactive Materials (NORM) (e.g., Carbon-14 and Tritium). The radiological search teams rely on automatic algorithms that can identify radiation anomalies in real-time. However, accurate identification of radioisotopes is a difficult task because large variations in factors, such as background conditions, poor energy resolution of radiation detectors, calibration shift, overlapping photo-peak energies, source strengths, and shielding conditions, make the identification

task complicated. Therefore, in addition to better hardware, a sophisticated computer algorithm is needed for the automatic detection of radioactive materials.

Automatic radioisotope detection algorithms can be roughly categorized into two types, classical condition-based, and machine learning-based approaches. In condition-based methods, an isotope can be identified by measuring the photo-peak energy information from the gamma spectra. This does not require any training method, and usually, physics-based rules were applied for identification. On the other hand, in machine learning-based approaches, gamma spectra and their respective isotope type need to be known in advance to train a predictive model. The trained model can then be used to estimate the probability of a radioisotope presence in an unseen environment.

Some of the condition based approaches [9] include simple library comparison [10,11], region of interest (ROI), template matching methods [12] and principal components analysis [13,14]. In the library comparison method, each photo-peak's centroid energy is considered, but not the area or branching ratio. A slight shift in detector response or calibration may result in inaccurate detections. In

* Corresponding author.

E-mail address: leehk@unm.edu (H.K. Lee).

the ROI method, one or multiple ROIs were selected from each nuclide. One of the major drawbacks of this method is that it fails if different nuclides contain overlapping ROIs. In the template matching method, a few example spectra of different radioisotopes were generated at varying strength and/or background conditions and then matched with a test spectrum. Condition-based approaches did not usually produce reliable results in real-time applications [9,15].

Machine Learning (ML) methods [16] have been studied for nearly three decades to address the shortcomings of condition-based approaches. Artificial Neural Network (ANN), Support Vector Machine (SVM), Decision Trees, Bayesian method, and Normalized Cut are some of the successfully applied ML methods [17–20]. Among these methods, ANNs, specifically, Fully Connected Neural Networks (FCNN) are studied extensively in recent years [21–25]. In this paper, we investigate a few variants of the ML methods suitable for radioisotope identification and propose an improved end-to-end solution.

The study is inspired by recent developments in the field of deep learning. Unlike FCNNs, deep learning methods usually need a large amount of training data to produce satisfactory results. Deep learning have achieved a significant gain in performance in the areas of computer vision [26,27], speech recognition [28], and text recognition [29] problems. The design strength of the deep learning method is its ability to exploit the presence of temporal/spatial relationships in data [30,31]. Convolutional Neural Network (CNN) and Recurrent Neural Network (RNN) are some of the state-of-the-art methods for modelling spatially/temporally auto-correlated data (i.e., visual imagery, audio, text, etc.) [16,30]. However, ML method such as FCNN, does not assume any relationship among input data points. This phenomenon makes FCNN inefficient in gamma spectroscopy techniques.

The main contribution of this paper is two-fold. First, we compare different state-of-the-art machine learning methods under controlled experimental conditions and discuss their strength and weakness. Second, we design a hybrid deep learning architecture that is well suited for spectral data interpretation, which is a fusion of traditional FCNN and deep learning models. Under similar experimental conditions, we show that the proposed method is superior to currently existing methods [32]. We have re-implemented the work of He et al. [21] as a baseline for this purpose.

2. Material and scope of this study

In this paper, we introduce Hybrid Neural Network (HNN) models for interpreting gamma-ray spectra using a supervised machine learning method. Specifically, we develop two hybrid neural networks: HCNN (hybrid convolutional neural network) and HRNN (hybrid recurrent neural network), combining the FCNN with CNN and RNN, respectively. These hybrid neural network models were compared with three traditional ML models of FCNN, RNN, and Gradient boosted decision trees (GBDT) to evaluate their performance. Moreover, we compare three different feature calculation methods that are relevant to gamma spectroscopy, namely, manual, semi-automatic, and automatic. In addition, we study the effects of the size of the training dataset, spectra acquisition time, and single/multi-isotope identification performance on the robustness and stability of the proposed and traditional ML models [32].

The gamma spectra dataset for this study was obtained from a publicly announced competition www.topcoder.com, which was organized by several US federal and non-federal agencies [33]. The dataset contained simulated radiological search data that would be typically generated by moving through the streets along a mid-

sized US city. For the simulations, the organizers employed Monte Carlo particle transport models [34] to generate data files in a time-series manner. A standard NaI(Tl) detector with 7.5% resolution at 661 keV, traveling in a search vehicle, was assumed. The moving speed of the detector varied between 1 and 13.4 m per second. Radioisotope type, strength, shielding conditions, and background conditions (like roadways, buildings, or structures) differed from case to case as well. In total, 9700 data files with publicly known ground truth were provided in the dataset [32].

The dataset contained six different types of radiation sources: highly enriched uranium (HEU), weapons-grade plutonium (WGPu), iodine (^{131}I , a medical isotope), cobalt (^{60}Co , an industrial isotope), technetium (^{99}mTc , a medical isotope), and a combination of ^{99}mTc and HEU. (A normalized set of energy spectra from the listed sources for both shielded and unshielded conditions are presented in Fig. 1.)

The sources represent both non-threatening medical/industrial isotopes and threatening weapon-producing isotopes. These radioisotopes contain more than one photo-peaks that overlap with one another. Besides, some of the photo-peaks that can be of interest appear at low energies (less than 200 keV). As the radiation shields can attenuate the low energy photons, those peaks are suppressed; which makes the task of automatic detection in real-time challenging.

3. Method: development of the hybrid ML-based RII algorithms

Simulated gamma-ray spectral data was used for training and testing the ML models. Features were extracted from gamma spectra using three different approaches based on their level of automation: manual, semi-automatic, and automatic. The training and testing data had different levels of shielding present. However, this data was collected from a competition [33] and the hosts did not disclose the exact shielding present for each source. Shielding was one of the 7 variables that was not revealed in the dataset. Therefore, the effects of these 7 variables were not studied independently. We evaluated different machine learning models using the same training-validation data split, so that we can compare the results of different models, irrespective of dataset variables.

The proposed two hybrid ML models, HCNN and HRNN, with the following ML models commonly used for automatic radioisotope identification: FCNN (He et al. implementation [21]), fine-tuned

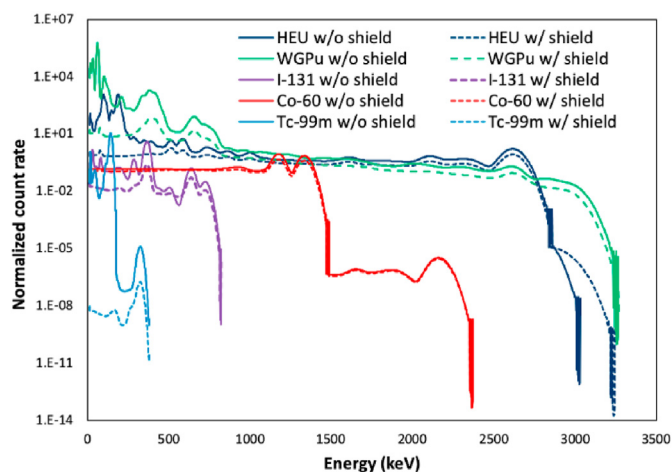


Fig. 1. Energy spectra of the five types of radioactive sources (HEU, WGPu, I-131, Co-60, and Tc-99 m) from a NaI(Tl) detector obtained using simulations by S. M. Galib (2019) [32].

RNN, and GBDT models. Below we describe these processes in relevant sections.

3.1. Training samples generation

Training spectra were generated using different data acquisition times. Acquisition time varies from 0.2 s–20 s. Multiple spectra were collected from each run (time-series data) of the detector. Fig. 2 demonstrates a schematic diagram of the training sample generation process. Approximately 60,000 training spectra were generated from 9700 time-series data available. About half of the spectra did not contain any source. The remaining of the spectra equally represented the six sources.

3.2. Feature extraction

Three sets of features (manual: PR, semi-automatic: DCT, and automatic: SC) were extracted from the gamma-spectra. These features were then fed into the ML models separately for analyzing their performances.

3.2.1. Peak ratios (PR)

In the Peak ratios (PR) method, 51 numerical features were calculated from the spectra based on the concept of peak-ratio in gamma spectroscopy. The generated data was based on NaI(Tl) detector. Bin counts of important energy values (keV) associated with the six isotopes were used to calculate peak-to-peak ratios and peak-to-compton ratios. Next, the 51 peak-ratio features were joined with 100-bin energy histogram to create 151 feature vectors for ML model training. We refer to this method as ‘manual,’ as the peak ratios are handcrafted features and depend on radioisotope type. Calculation of these features does not increase the computational burden significantly but still helps in extracting meaningful information from a gamma spectrum. Reference gamma-energy was determined such that the energy peak would appear in both shielded and unshielded conditions for any specific source. The peak energy values are listed in Table 1.

3.2.2. Discrete cosine transform (DCT)

DCT converts a signal into the frequency domain, and the transformation kernel is a cosine function. The advantage of DCT is that it can pack the energy of the spatial sequence into a few frequency coefficients. DCT has been successfully used in radioisotope

detection algorithms [21]. In total, 128 feature vectors were extracted from 100-channel gamma spectra using DCT. We refer to this method as ‘semi-automatic,’ as one still needs to find out which transform method may work well for gamma spectroscopy.

3.2.3. Spectrum counts (SC)

SC features are the number of counts in each channel of the gamma spectra. These features can be interpreted as raw data as no explicit feature calculation was carried out on this method. For the experiments, 100 channel spectra were used, and SC features were fed to ML models after the normalization and scaling of the data. We refer to this method as ‘automatic,’ as the features are essentially raw data from the spectrum.

3.3. Machine learning models

Three state-of-the-art models (FCNN, RNN, and GBDT) and two newly developed models (HCNN and HRNN) were tested in this study and compared. Four of the classifiers were neural network based, and the other one (GBDT) was decision tree based. Below a short description of the classifiers is presented.

3.3.1. Fully-connected neural network (FCNN)

A fully-connected Neural Network (FCNN) is the classical form of neural networks. Artificial neurons are arranged in a layer-wise manner, and each neuron in one layer connects to all neurons in the next layer. An FCNN with only one hidden layer can approximate any non-linear function. Typically, there is one input layer, one output layer, and there can be multiple hidden layers. In this study, we re-implemented an FCNN model adapted from the work of He et al. [21]. The FCNN consists of one hidden layer with eight neurons, and we considered this as a baseline model.

3.3.2. Convolutional neural network (CNN)

CNNs are a regularized version of multi-layer neural networks [16]. This can extract abstract representations of input data that contains spatial or temporal relationship, and they are also known as ‘shift-invariant’ or ‘space invariant’ neural networks. CNNs work on successive convolution operations and popular in image recognition problems where 2D/3D data are used [35,36]. However, this model can operate on n-dimensional data and thus applicable to 1D detector data for high-level feature extraction.

3.3.3. Recurrent neural network (RNN)

Unlike FCNN, neurons in RNNs exhibit temporal connections, which makes them useful for sequence learning applications [37–41]. We implemented an RNN based on long short-term memory (LSTM) [42] cells. LSTM provides a solution for the vanishing gradient problem in RNNs. The RNN has 2-hidden layers before the classification layer. Hyperparameters, such as the number of hidden layers and LSTM cells, were optimized experimentally.

3.3.4. Gradient boosted decision trees (GBDT)

The gradient boosted version of decision trees (GBDT) is an ensemble of several weak decision tree models. GBDT is one of the most popular algorithms used in ML and a possible candidate for gamma spectroscopy [43,44]. However, like FCNN, GBDT does not assume any sequential or temporal relationship between input data points.

3.3.5. Hybrid convolutional neural network (HCNN)

In the HCNN model, convolutional feature vectors were extracted from the input data by a 2-layer CNN. Next, these features were added to the original input features to produce a more

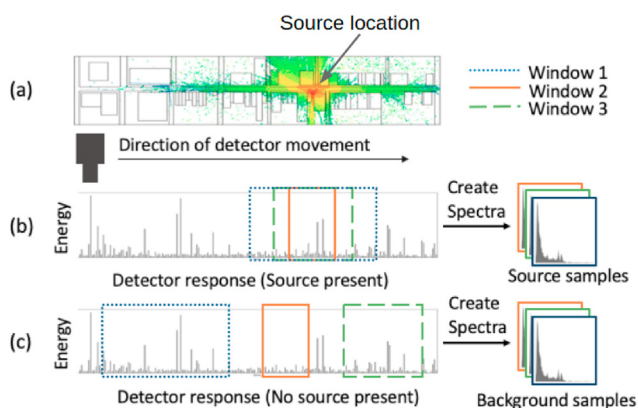


Fig. 2. The process of training spectra generation from time-series detector data. (a): an illustrative diagram of the experimental setup. It contains position information of the source. Top part shows a heat map of the source positioned along a street. The bottom part shows the direction of the detector movement. (b) and (c): the time-series detector data generated by the detector in (a). The x-axis is time and dotted boxes represent the time span of data collected for ML model training.

Table 1

List of radioisotopes studied, their significant peak energies for PR feature calculation, and search data file (samples).

ID	Source type	Ref. Energies (keV)	Other energies (keV)	No. Of samples
0	Background	—	—	4900
1	HEU	511, 585	17, 97, 187, 2615	800
2	WGPu	381, 407	33, 61, 77, 101, 207, 653	800
3	131I	365	31, 81, 185, 285, 637	800
4	60Co	1173, 1333	—	800
5	99 mTc	141	19, 45, 321	800
6	HEU +99 mTc	141, 511, 585	17, 19, 45, 97, 187, 321	800

extensive feature space. Feature vectors were then fed to a 2-layer FCNN, which produced final predictions. The model was trained end-to-end. Fig. 3 demonstrates the schematic diagram of hybrid neural network architecture, which consist of input features, convolution features, layers of FCNN neural networks.

3.3.6. Hybrid recurrent neural network (HRNN)

HRNN is mostly similar to HCNN, except that it uses RNN layers instead of convolutional layers for feature extraction. A two-layer RNN with LSTM cells was employed on this architecture, as shown in Fig. 3.

3.4. Training and validation

We divided the dataset into training, validation, and testing set in the ratio of 80%–10%–10% using random splitting. All the sets contained a balanced percentage of radioisotope samples. Neural network models were trained using categorical cross-entropy loss function. Adam [45] optimizer was employed to minimize training loss. Furthermore, batch normalization [46] was applied to train the model faster. Moreover, dropout [47] was utilized to reduce the overfitting of the model. For the GBDT model, hyperparameters, such as learning rate, number of trees, number of leaves, max-depth, and a few others, were optimized for the experiments.

3.5. Testing

For testing, sliding window method was used to predict the probability of a source. Windows were taken at multiple acquisition times. This multi-window prediction strategy usually improves the

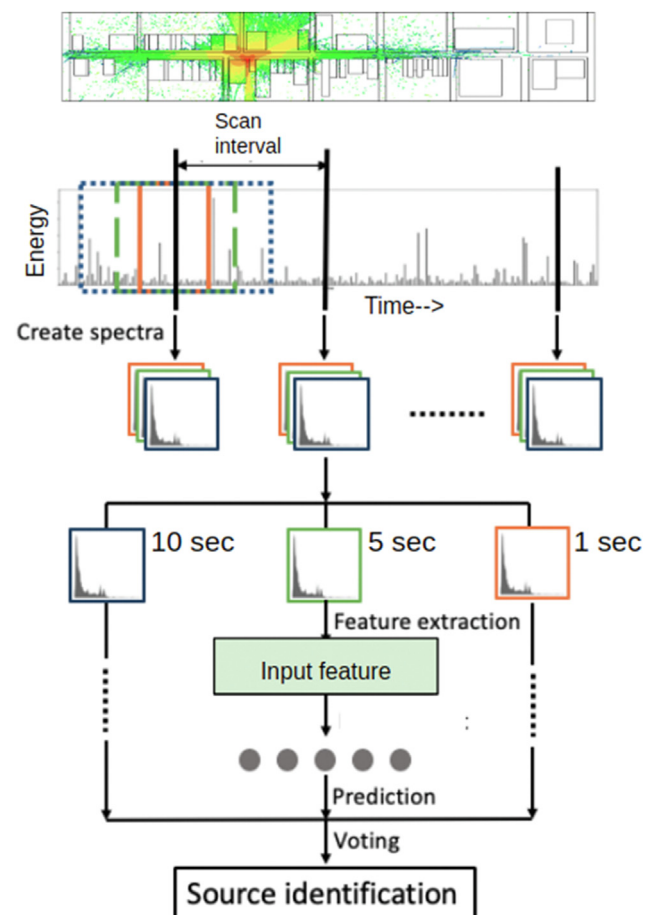
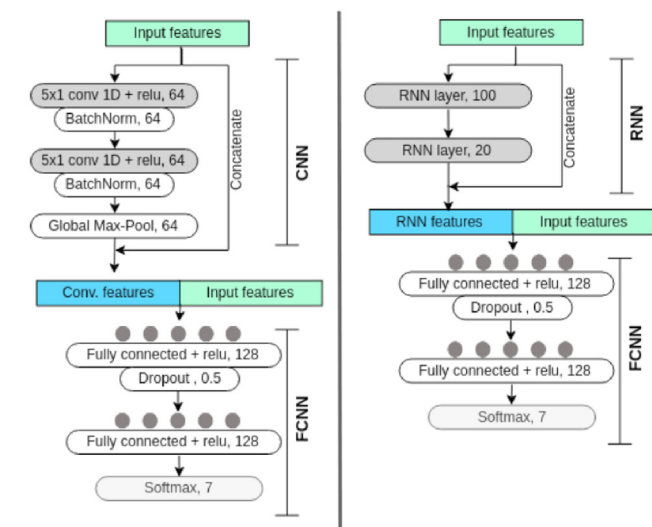
performance of ML algorithms. However, inference time also increases with this method. Fig. 4 demonstrates a schematic diagram of the testing procedure.

3.6. Implementation

The algorithm was implemented using Python programming language. Keras [48] deep learning library was used to construct the neural network models. LightGBM [49] library was employed for GBDT model training.

3.7. Evaluation metric

The performance of the methods was quantified using the F1 measure. F1 measure is a balance between precision and recall and is commonly used in multi-class classification problems [50] as:

**Fig. 4.** Multi-window prediction and voting strategy for radioisotope identification.**Fig. 3.** Schematic diagram of hybrid neural network architectures: HCNN (left) and HRNN (right) with hybrid neural network architecture consisting of features and network layers.

$$\text{Precision} = \frac{\text{True positive}}{\text{True positive} + \text{False positive}} \quad (1)$$

$$\text{Recall} = \frac{\text{True positive}}{\text{True positive} + \text{False negative}} \quad (2)$$

$$\text{F1} = \frac{2\text{precisionrecall}}{\text{precision} + \text{recall}} \quad (3)$$

Precision and Recall is based on True Positive (TP), False Positive (FP) and False Negative (FN). The threshold is 0.5, which is applied to the ML model output probability to determine TP, FP or FN. F1 measure can range from 0 to 1, where 1 means perfect precision and recall. Specifically, the macro-F1 metric was used [50]. It assigns equal importance to every class during evaluation despite the class imbalance.

Model training was repeated 20 times to calculate the estimated variance of the testing results. ML models may exhibit some randomness in output when re-training with the same data with the same hyperparameters (if random seed is not fixed). A weak model will show more randomness than a robust model. We re-ran the experiments 20 times to evaluate the randomness/variance of the models.

4. Results and discussion

The chosen experimental conditions and the five ML model performance were discussed in the following sections.

4.1. Effect of train dataset size

An ML model robustness can be evaluated by measuring its performance on limited training data conditions. A robust model accuracy should not decrease significantly with a decrease in training data samples. Moreover, a stable model is one that demonstrates less variance in prediction performance among different training sessions. Fig. 5 illustrates the mean F1 score of the 5 models when trained with varying training dataset sizes (i.e., 5%, 10%, 20%, 40%, and 80% of training dataset).

The models were trained and evaluated using 5-s spectra. At 80% training size, all models showed comparable accuracy. We observe that HCNN and HRNN models showed high F1 score at low train percentages and achieved 5–20% improvement, compared to the other three models when trained with only 5% of training data. The standard deviation for the hybrid models was below 1% under difficult training conditions (i.e., low train percentages). However, RNN models showed high standard deviation, compared to others, which implies that they are not very stable predictive models.

When we compared the three feature sets, DCT and PR sets showed higher accuracy for all models, compared to SC features. DCT and PR sets provided 2–8% improvement over SC feature at 5%

training data conditions for all the models. This implies that semi-automatic or manual feature extraction does help in the generalization of ML models.

4.2. Effect of spectra acquisition time

Assuming a moving detector, a low data acquisition time (i.e., 0.2 s) may result in weak source signal, whereas a high acquisition time (i.e., 20 s) may suppress the signals.

Fig. 6 demonstrates a comparison among the models at varying data acquisition times. HCNN and HRNN models showed higher accuracy than the other models in most of the cases. At 0.2 s acquisition time, HNN models achieved 2–12% improvement in F1 score than the other three models for all feature sets. At 20 s, we observed 1–5% improvement of hybrid models. HCNN performed better than HRNN under most of the conditions.

We also observed that PR features improved the performance of all models than the other two feature sets. PR and DCT features achieved a close 3–5% gain in F1 score at 0.2s spectra conditions, compared to SC. All experiments were carried out using 80% train data.

4.3. Run time

Fig. 7 demonstrates the training and testing times for all five models. FCNN models were the fastest to train and test primarily because of their relatively simple architecture. RNN and HRNN took almost 120 times the time it took to train the FCNN models. HCNN and GBDT models were five times slower than FCNN models during training. During testing, the neural network model's run time remained constant, even with increases in training dataset size, and was usually faster than GBDT models. HCNN was two times faster than HRNN during test time. We observed a rise in inference time for GBDT models as the training data increased. This is explainable as more data means more complex conditions can be fitted with the GBDT model, and the trees grow more in depth with more states, which, in turn, increases the run time.

4.4. Multi-class classification performance

Fig. 8 demonstrates F1 score for each individual radioisotope in the dataset for all five models. Models were trained using 80% of training data, 5 s spectra with SC feature set. We observed a relatively high accuracy for background, I-131, and Co-60 (ID 0, 3 and 4, respectively) radioisotopes, compared to the other four combinations. Lower accuracy for HEU, WGPu, Tc-99m, and HEU + Tc-99m can be explained by analyzing their most active peak energies. These four radioisotopes have high activity peaks below 200 keV, which can be greatly affected by shielding conditions. Therefore, low peak energy isotopes are relatively difficult to detect.

When compared, the hybrid models achieved a higher F1 score than the other models, especially for difficult radioisotopes and

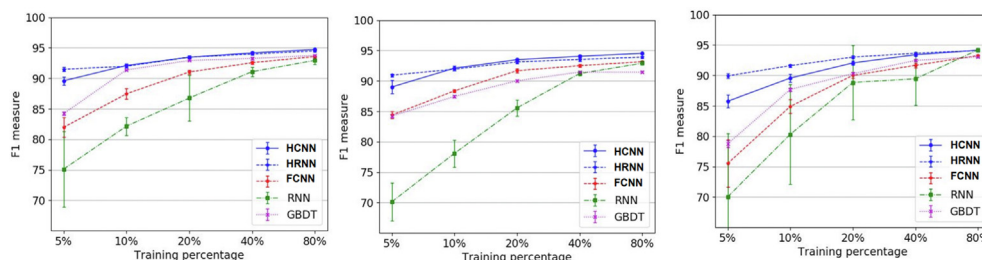


Fig. 5. F1 score (%) on test dataset predicted by five ML models at different training percentages of full data for feature set: (left) PR, (middle) DCT, (right) SC.

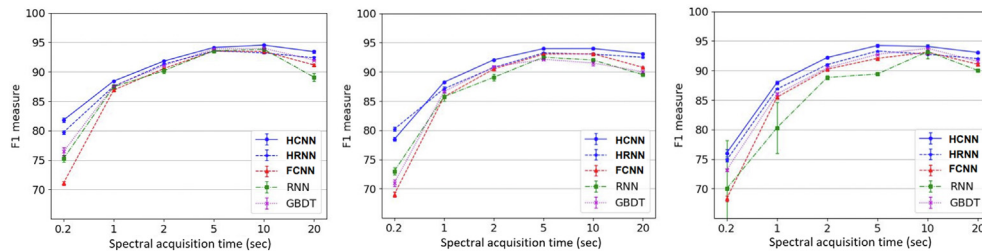


Fig. 6. F1 score (%) on test dataset predicted by five ML models at different spectra acquisition times for feature set: (left) PR. (middle) DCT. (right) SC.

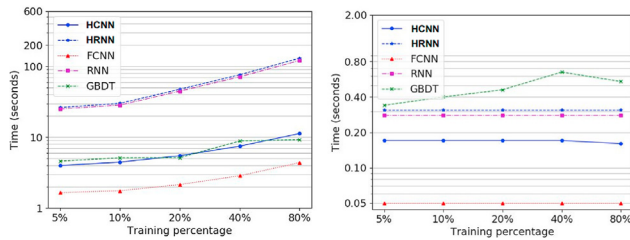


Fig. 7. Run-time of the five models using 5s spectra with increasing train data percentage of full data: (left) training time. (right) testing time.

Table 2

Effect of data augmentation for HCNN model on test dataset.

No. Of windows used	Acquisition time (s)	F1 score (%)
1	5	92.23 ± 0.68
2	5, 10	92.71 ± 0.32
3	5, 10, 20	93.04 ± 0.11
4	2, 5, 10, 20	93.27 ± 0.05
5	1, 2, 5, 10, 20	93.33 ± 0.08

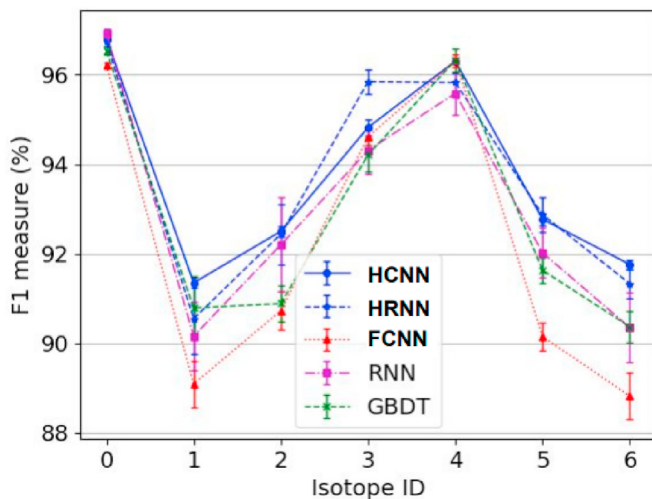


Fig. 8. F1 score (%) on test data for 7-class classification (using isotope ID: 0-Background, 1-HEU, 2-WGpu, 3-131I, 4-60Co, 5-99mTc, and 6- HEU + 99 mTc) by five models using 5s spectra and SC feature set.

combinations (HEU, WGPu, Tc-99 m, and HEU + Tc-99 m). For a multi-isotope scenario (ID 6: HEU + Tc-99 m), the hybrid models achieved at least 2% improvement over the other three models. Both hybrid models performed comparably with a lower standard deviation than the other model. Moreover, for ID 0, 3, and 4, the performance of all the models was closely comparable.

4.5. Effect of multi-window testing

Table 2 demonstrates the result of multi-window prediction using the HCNN model. Using five windows at varying acquisition times, prediction results were improved by more than 1%, compared to using only 5s window spectra. Moreover, the uncertainty of the predictions became lower as the number of windows were increased.

4.6. Effect of background

The result of the background was important considering the nature of the data and study. The study was performed assuming a moving detector capable of detection if there are any radiation anomalies. If the background detection accuracy is not high enough, it will produce a large amount of false positives. The threshold to determine any radionuclide and the background was set to 0.5. This threshold selection might not be optimal, but for simplicity we kept it the same for all our experiments.

In summary, we studied five state-of-the-art ML methods and three sets of feature engineering methods for automated radio-isotope detection. Hybrid neural networks were developed based on FCNN, RNN, and CNN architectures. It was observed that the hybrid models were more accurate and robust than the traditional models at a wide range of parameter choices. Between the hybrid models, HCNN showed comparable or better accuracy than the HRNN model for most of the cases, while HCNN ran two times faster than HRNN. When the hybrid models were evaluated based on the training dataset size and spectra acquisition time, they showed 2–12% improvement in challenging prediction scenarios, compared to the best traditional models (FCNN). Moreover, hard radioisotope combinations, such as multi-isotopes (i.e., HEU + Tc-99 m) and their parent isotopes, were detected 1–2% more accurately with hybrid models. With data augmentation, the HCNN model was able to achieve 93.33% F1 score in test data. Overall, HCNN architecture was more accurate and efficient among the models studied.

5. Conclusions

In this study, we have developed hybrid neural network architectures, which is a fusion of traditional feed-forward neural network and modern deep learning architectures. Experiments show that hybrid ML models are promising methods for real-time applications. Deep learning models such as CNN or RNN may not produce maximum possible accuracy alone due to limited data, however, when combined with traditional methods, hybrid models outperform their base architectures.

One of the limitations of this study was that only simulated spectra were used for training and testing. The algorithm needs

further verification using real-detector-measured spectra. Besides, for best performance, handcrafted feature calculation remains important. Future ML models are expected to be capable of eliminating the explicit feature calculation step as this requires both expert knowledge and extra computation cost. This developed algorithm can be trained and validated further subjected to availability of the new dataset with more sources available.

Overall, the HCNN model was found to work best for the automated radioisotope classification task. This implies that the deep learning method, such as CNN, is a useful and promising technique for gamma-ray spectroscopy. This also demonstrates that ML models tailored to a specific problem often leads to a better generalization of the algorithms.

Declaration of competing interest

The authors declare that they have no known competing financial interests or personal relationships that could have appeared to influence the work reported in this paper.

Acknowledgments

No funding to declare. Thanks to detecting radiological threats in urban areas - challenge. <https://www.topcoder.com/challenges/30085346> for sharing the necessary data for this study.

Nomenclature

ANN	Artificial neural network
CNN	Convolutional neural network
DCT	Discrete cosine transform
FCNN	Fully-connected neural network
GBDT	Gradient boosted decision trees
HCNN	Hybrid convolutional neural network
HRNN	Hybrid recurrent neural network
ML	Machine learning
PR	Peak ratio
RNN	Recurrent neural network
SC	Spectrum counts

References

- [1] D. Connor, P.G. Martin, T.B. Scott, Airborne radiation mapping: overview and application of current and future aerial systems, *Int. J. Rem. Sens.* 37 (24) (2016) 5953–5987.
- [2] Yukihisa Sanada, Tatsuo Torii, Aerial radiation monitoring around the Fukushima dai-ichi nuclear power plant using an unmanned helicopter, *J. Environ. Radioact.* 139 (2015) 294–299.
- [3] Mucci Anthony, Drone Tours in Security Systems, US Patent App, April 28 2016, 14/516,651.
- [4] Yoshinori Uekusa, Hiromi Nabeshi, Rika Nakamura, Tomoaki Tsutsumi, Akiko Hachisuka, Rieko Matsuda, Reiko Teshima, Surveillance of radioactive cesium in domestic foods on the Japanese market (fiscal years 2012 and 2013). *Shokuhin eiseigaku zasshi*, J. Food Hyg. Soc. Jpn. 56 (2) (2015) 49–56.
- [5] D.R. Rangaswamy, J. Sannappa, E. Srinivasa, Estimation of radiological dose from radon, thoron and their progeny levels in the dwellings of shivamogga district, Karnataka, India, in: *Proceedings of the Thirty-Third IARP International Conference on Developments towards Improvement of Radiological Surveillance at Nuclear Facilities and Environment: Book of Abstracts*, 2018.
- [6] Masahiro Hosoda, Kazumasa Inoue, Mitsuaki Oka, Yasutaka Omori, Kazuki Iwaoka, Shinji Tokonami, Environmental radiation monitoring and external dose estimation in aomori prefecture after the Fukushima daiichi nuclear power plant accident, *保健物理* 51 (1) (2016) 41–50.
- [7] Miyuki Sasaki, Yukihisa Sanada, Estiner W. Katengeza, Akio Yamamoto, New method for visualizing the dose rate distribution around the Fukushima daiichi nuclear power plant using artificial neural networks, *Sci. Rep.* 11 (1) (2021) 1–11.
- [8] Huseyin Sahiner, Gamma Spectroscopy by Artificial Neural Network Coupled with MCNP, PhD thesis, 2017.
- [9] Tom Burr, Michael Hamada, Radio-isotope identification algorithms for NaI γ spectra, *Algorithms* 2 (2009) 339–360.
- [10] Miltiadis Alamaniotis, Heifetz Alexander, Apostolos C. Raptis, Lefteri H. Tsoukalas, Fuzzy-logic radioisotope identifier for gamma spectroscopy in source search, *IEEE Trans. Nucl. Sci.* 60 (4) (2013) 3014–3024, 8.
- [11] M.T. Batdorf, W.K. Hensley, C.E. Seifert, L.J. Kirihaara, L.E. Erikson, D.V. Jordan, Isotope identification in the GammaTracker handheld radioisotope identifier, in: *2009 IEEE Nuclear Science Symposium Conference Record (NSS/MIC)*, IEEE, 2009, pp. 868–872, 10.
- [12] Dean J. Mitchell, Lee T. Harding, GADRAS Isotope ID User's Manual for Analysis of Gamma-Ray Measurements and API for Linux and Android. Technical Report, Sandia National Laboratories (SNL), Albuquerque, NM, and Livermore, CA (United States), 2014, 5.
- [13] R.C. Runkle, M.F. Tardiff, K.K. Anderson, D.K. Carlson, L.E. Smith, Analysis of spectroscopic radiation portal monitor data using principal components analysis, *IEEE Trans. Nucl. Sci.* 53 (3) (2006) 1418–1423, 6.
- [14] David Boardman, Mark Reinhard, Alison Flynn, Principal component analysis of gamma-ray spectra for radiation portal monitors, *IEEE Trans. Nucl. Sci.* 59 (1) (2012) 154–160.
- [15] C.J. Sullivan, S.E. Garner, M. Lombardi, K.B. Butterfield, M.A. Smith-Nelson, Evaluation of key detector parameters for isotope identification, in: *2007 IEEE Nuclear Science Symposium Conference Record*, IEEE, 2007, pp. 1181–1184.
- [16] Ian Goodfellow, Yoshua Bengio, Aaron Courville, Yoshua Bengio, *Deep learning*, 1, MIT press Cambridge, 2016.
- [17] Yan T. Yang, Barak Fishbain, Dorit S. Hochbaum, Eric B. Norman, Erik Swanberg, The supervised normalized cut method for detecting, classifying, and identifying special nuclear materials, *Inf. J. Comput.* 26 (1) (2013) 45–58.
- [18] S. Salaymeh, R. Jeffcoat, Radioisotope Identification of Shielded and Masked Snm Rdd Materials. Technical Report, Savannah River Site (SRS), 2010.
- [19] T.R. Twomey, A.J. Caffrey, D.L. Chichester, Nondestructive Identification of Chemical Warfare Agents and Explosives by Neutron Generator-Driven Pgnaa. Technical Report, Idaho National Laboratory (INL), 2007.
- [20] Tom Burr, Michael Hamada, Radio-isotope identification algorithms for nai γ spectra, *Algorithms* 2 (1) (2009) 339–360.
- [21] Jianping He, Xiaobin Tang, Pin Gong, Peng Wang, Liangsheng Wen, Xi Huang, Zhenyang Han, Yan Wen, Le Gao, Rapid radionuclide identification algorithm based on the discrete cosine transform and BP neural network, *Ann. Nucl. Energy* 112 (1–8) (2018) 2.
- [22] Changfan Zhang, Gen Hu, Fei Luo, Yongchun Xiang, Ge Ding, Chengsheng Chu, Jun Zeng, Ze Rende, Qingpei Xiang, Identification of SNM based on low-resolution gamma-ray characteristics and neural network, *Nucl. Instrum. Methods Phys. Res. Sect. A Accel. Spectrom. Detect. Assoc. Equip.* 927 (155–160) (2019), 5.
- [23] M. Kamuda, J. Stinnett, C.J. Sullivan, Automated isotope identification algorithm using artificial neural networks, *IEEE Trans. Nucl. Sci.* 64 (7) (2017) 1858–1864, 7.
- [24] Elsayed K. Elmaghraby, M. Tohamy, M.N.H. Comsan, Determination of isotopes activity ratio using gamma ray spectroscopy based on neural network model, *Appl. Radiat. Isot.* 148 (19–26) (2019) 6.
- [25] C. Bobin, O. Bichler, V. Lourenço, C. Thiam, M. Thévenin, Real-time radionuclide identification in γ -emitter mixtures based on spiking neural network, *Appl. Radiat. Isot.* 109 (405–409) (2016), 3.
- [26] Alex Krizhevsky, Ilya Sutskever, Geoffrey E. Hinton, Imagenet classification with deep convolutional neural networks, in: *Advances in Neural Information Processing Systems*, 2012, pp. 1097–1105.
- [27] Olga Russakovsky, Deng Jia, Hao Su, Jonathan Krause, Sanjeev Satheesh, Sean Ma, Zhiheng Huang, Andrej Karpathy, Aditya Khosla, Michael Bernstein, Alexander C. Berg, Li Fei-Fei, ImageNet large scale visual recognition challenge, *Int. J. Comput. Vis.* 115 (3) (2015) 211–252, 12.
- [28] Alex Graves, Abdel-rahman Mohamed, Geoffrey Hinton, Speech recognition with deep recurrent neural networks, in: *Acoustics, Speech and Signal Processing (Icassp)*, 2013 IEEE International Conference on, IEEE, 2013, pp. 6645–6649.
- [29] Karl Moritz Hermann, Tomas Kocisky, Edward Grefenstette, Lasse Espeholt, Will Kay, Mustafa Suleyman, Phil Blunsom, Teaching machines to read and comprehend, in: *Advances in Neural Information Processing Systems*, 2015, pp. 1693–1701.
- [30] G. Daniel, F. Ceraudo, O. Limousin, D. Maier, A. Meuris, Automatic and real-time identification of radionuclides in gamma-ray spectra: a new method based on convolutional neural network trained with synthetic data set, *IEEE Trans. Nucl. Sci.* 67 (4) (2020) 644–653.
- [31] Mark Kamuda, Jacob Stinnett, C.J. Sullivan, Automated isotope identification algorithm using artificial neural networks, *IEEE Trans. Nucl. Sci.* 64 (7) (2017) 1858–1864.
- [32] Shaikat Mahmood Galib, Applications of Machine Learning in Nuclear Imaging and Radiation Detection, 2019.
- [33] Detecting radiological threats in urban areas - challenge, Accessed on 01/05/2021, <https://www.topcoder.com/challenges/30085346>.
- [34] Scale — ornl, Accessed on 01/05/2021, <https://www.ornl.gov/scale>.
- [35] Shaikat M. Galib, Hyoun K. Lee, Christopher L. Guy, Matthew J. Riblett, Geoffrey D. Hugo, A fast and scalable method for quality assurance of deformable image registration on lung ct scans using convolutional neural networks, *Med. Phys.* 47 (1) (2020) 99–109.
- [36] Wei Ouyang, Casper F. Winsnes, Hjelmar Martin, Anthony J. Cesnik, Lovisa Åkesson, Hao Xu, Devin P. Sullivan, Shubin Dai, Jun Lan, Jinmo Park, et al., Analysis of the human protein atlas image classification competition, *Nat. Methods* 16 (12) (2019) 1254–1261.

- [37] Karl Moritz Hermann, Tomáš Kočiský, Edward Grefenstette, Lasse Espeholt, Will Kay, Mustafa Suleyman, Phil Blunsom, Teaching Machines to Read and Comprehend, 2015, pp. 1–9.
- [38] Ilya Sutskever, Oriol Vinyals, V Le Quoc, Sequence to sequence learning with neural networks, in: *Advances in Neural Information Processing Systems*, 2014, pp. 3104–3112.
- [39] Alex Graves, Greg Wayne, Ivo Danihelka, Neural Turing Machines, 2014 arXiv preprint arXiv:1410.5401.
- [40] Tomas Mikolov, Kai Chen, Greg Corrado, Jeffrey Dean, Efficient Estimation of Word Representations in Vector Space, 2013 arXiv preprint arXiv:1301.3781.
- [41] Alex Graves, Generating Sequences with Recurrent Neural Networks, 2013 arXiv preprint arXiv:1308.0850.
- [42] S. Hochreiter, J. Schmidhuber, Long short-term memory, *Neural Comput.* 9 (8) (11 1997) 1735–1780.
- [43] P.M. Saz Parkinson, H. Xu, P.L.H. Yu, D. Salvetti, M. Marelli, A.D. Falcone, CLASSIFICATION and RANKING OFFERMITAT GAMMA-RAY sources from the 3fgl CATALOG using machine learning techniques, *Astrophys. J.* 820 (1) (mar 2016), 8.
- [44] Barzilov Alexander, Ivan Novikov, Material classification by analysis of prompt photon spectra induced by 14-mev neutrons, *Physics Procedia* 66 (2015) 396–402. The 23rd International Conference on the Application of Accelerators in Research and Industry - CAARI 2014.
- [45] Diederik Kingma, Ba Jimmy, Adam: A Method for Stochastic Optimization, 2014 arXiv preprint arXiv:1412.6980.
- [46] Sergey Ioffe, Christian Szegedy, Batch Normalization: Accelerating Deep Network Training by Reducing Internal Covariate Shift, 2015 arXiv preprint arXiv:1502.03167.
- [47] Nitish Srivastava, Geoffrey E. Hinton, Alex Krizhevsky, Ilya Sutskever, Ruslan Salakhutdinov, Dropout: a simple way to prevent neural networks from overfitting, *J. Mach. Learn. Res.* 15 (1) (2014) 1929–1958.
- [48] François Chollet, et al., Keras. <https://keras.io>, 2015.
- [49] Dehua Wang, Yang Zhang, Yi Zhao, Lightgbm: an effective mirna classification method in breast cancer patients, in: *Proceedings of the 2017 International Conference on Computational Biology and Bioinformatics, ICCBB, New York, NY, USA, 2017*, pp. 7–11, 2017. ACM.
- [50] Juri Opitz, Sebastian Burst, Macro F1 and Macro F1, 2019 arXiv preprint arXiv: 1911.03347.